A Coordinated Control Architecture With Inverter-Based Resources and Legacy Controllers of Power Distribution System for Voltage Profile Balance

Arun Suresh, *Student Member, IEEE*, Robin Bisht, *Student Member, IEEE*, and Sukumar Kamalasadan, *Senior Member, IEEE*

***Abstract*—In this article, a coordinated control architecture is proposed that utilizes inverter-based distributed energy resources (DERs) and legacy controllers such as voltage regulators in a power distribution system and coordinates the reactive power support such that the voltage balance at a particular node of interest can be achieved. The approach is developed based on the alternating direction method of multipliers and the optimal control framework, where a primary control loop is used to provide the necessary reactive power set point to mitigate the voltage deviation and a secondary control loop is used to balance the reactive power from multiple devices such as DERs. The methodology is tested on the IEEE 123-bus distribution feeder with multiple three-phase DERs in coordination with a voltage regulator. It has been observed that the proposed architecture can reduce regulator tap operation, improve the voltage deviation (at least by 20%), and, at the same time, mitigate the negative effect of the reverse operation of the regulators.**

***Index Terms*—Distributed control framework, inverter-based resources (IBRs), voltage coordination, voltage profile improvement, voltage regulator.**

I. Introduction

POWER distribution systems with high penetration of DERs offer significant merits in the form of the ability to manage voltage at different points due to inverter-based resources (IBRs), reduction in losses due to the local generation and consumption, sustainable generation of power, and contributing toward carbon neutrality especially if DERs are renewable energy based. However, one critical aspect that is coordinated voltage profile balance in the distribution system where the IBRs and legacy controllers are to be coordinated well to manage the voltage profile throughout the grid has been a very important point of research recently. High proliferation of DERs can impact low- and medium-voltage systems even though DERs can provide distributed power and, thus, can be used to serve local loads. For example, widely varying DERs with energy resources can cause problems in voltage regulation in distribution networks. One way of implementing the DERs is in the form of a microgrid considering load generation balance and grid connectivity. An overview of microgrid controls with IBRs is discussed in [1].

Conventional approaches that have been presented in the literature for distributed and decentralized control solutions are based on optimization frameworks, including mixed-integer convex or nonconvex variants. Such methodologies are, in general, time consuming when compared to the control set points required for managing IBRs. For example, approaches mentioned in [2]–[4] can only be implemented within a time frame that spans from minutes to hours. Thus, such approaches are not feasible in real-life scenarios to manage the IBR-based resources and use them for coordination with the legacy devices and controllers when the dynamics are within milliseconds or seconds.

Newaz *et al.* [5] present the coordinated voltage control of the distribution system based on a sensitivity-based approach along with an electrical distance metric calculation. The control algorithm is dependent on the electrical distance calculation and the inverse of the Jacobian-based sensitivity matrix. However, it has been noted that the electrical distance measure and calculation cannot provide exact power transfer, especially with reactive power. Distributed approaches that can be implemented in the field have been attempted in recent works. One of the main approaches involves the alternating direction method of multipliers (ADMM) based on distributed optimization. For example, in [6], a methodology to optimally set the reactive power from DERs has been proposed that coordinates the optimal

Manuscript received 31 December 2021; revised 1 April 2022; accepted 11 May 2022. Date of publication 14 June 2022; date of current version 25 August 2022. Paper 2021-IACC-1428.R1, presented at the 2020 IEEE International Conference on Power Electronics, Drives and Energy Systems, Jaipur, India, Dec. 16–19, and approved for publication in the IEEE Transactions on Industry Applications by the Industrial Automation and Control Committee of the IEEE Industry Applications Society. This work was supported in part by the U.S. Department of Energy's Office of Energy Efficiency and Renewable Energy and the Solar Energy Technologies Office under Grant DE-EE0008774 and in part by the National Science Foundation under Grant ECCS-1810174. *(Corresponding author: Sukumar Kamalasadan.)*

Arun Suresh was with the Department of Electrical and Computer Engineering, University of North Carolina at Charlotte, Charlotte, NC 28223 USA. He is now with Hitachi Energy, Raleigh, NC 27606 USA (e-mail: asuresh4@uncc.edu).

Robin Bisht and Sukumar Kamalasadan are with the Department of Electrical and Computer Engineering, University of North Carolina at Charlotte, Charlotte, NC 28223 USA (e-mail: rbisht@uncc.edu; skamalas@uncc.edu).

Color versions of one or more figures in this article are available at https://doi.org/10.1109/TIA.2022.3183030.

Digital Object Identifier 10.1109/TIA.2022.3183030

power flow framework with the ADMM. However, the real-time implementation and the feasibility of the approach to run with a faster time frame are questionable.

Another relevant approach mentioned in [7] demonstrates an optimal decentralized voltage control framework for IBRs. The approach uses a local optimization framework based on offline sensitivity studies to avoid computational complexity, and a 10-min interval optimization approach is designed. Even though the approach is feasible, the solutions depend much on offline calculations and their accuracy. Moreover, the time frame is not suitable for real-time implementation. A better feasible approach is presented in [8], where a distributed voltage control framework is proposed considering communication issues, time-varying adaptations, and reduced computational complexity. However, field implementation of this approach is not presented; thus, feasibility is a big concern. In [9], a real-time coordinated voltage control framework with photovoltaic (PV) inverters and energy storage is proposed. The approach is applied to the weak grid and high PV penetration scenarios. The approach is a centralized controller based on field measurements. Even though field implementation is possible, coordination of multiple DERs is questionable.

For field implementation and consideration for this, any control architecture should be tested in conjunction with the primary control of the IBRs and the legacy devices. Current methodologies proposed control architecture based on two scenarios. The first one is a local or decentralized control framework that considers distributed generators (DGs) locally and without any coordination [10] or with minimal coordination [11] with other DGs. Such approaches are easier to implement and have a faster response time. However, while considering voltage profile management, coordination between multiple DERs and legacy devices is critical. Alobeidli and Moursi [12], Miret *et al.* [13], and Viawan and Karlsson [14] have attempted the coordinated control based on secondary voltage management and inverter control. However, the approach uses the one-point information from the grid to regulate the DER set points. One main contribution that has been made in the recent past is the measurement-based modeling of the power grid considering the DERs and other devices based on the ADMM [15], [16]. In this approach, multiple-input multiple-output (MIMO) frequency-domain models can be derived based on the ADMM. The advantage of this approach is that it provides the input–output sensitives based on measurements (reducing complexities in sensitivity calculations) and, at the same time, provides a state-space representation of the system considering DERs and controllers.

Abdelrazek *et al.* [17] and Ahmed and Kamalasadan [18] have demonstrated how the field DERs can be coordinated to provide distributed control without a communication framework. The approach mentioned in these references has been implemented in the local utility and is currently deployed fleetwide. This shows that the coordinated control that works with both the primary- and secondary-level controllers can be developed and field implemented. However, in the presence of multiple DERs, the group of DERs should manage the voltage in a distributed manner. At the same time. the voltage control should be coordinated with the legacy controllers such as voltage regulators. Distributed management and control algorithms should consider the interaction between units. To have the control approach distributed, a distributed model is required either through optimization or based on clustering that gives set points and in tandem develops dynamics included in the control objective, or one should use the distributed control approaches such as model-predictive control framework where dynamic optimization and control objectives are included in one objective. Several works related to distributed control have been proposed in the recent past [19]–[24]. However, coordinated distributed control architecture is imperatively required for the voltage control of the DER integrated distribution system. In our earlier work, local inverter controllers for single-phase inverters for grid-tied operations have been designed and implemented that can be deployed in the field [25]. Furthermore, Suresh *et al.* [26] demonstrated the ADMM-based DER control considering voltage at one particular node of interest in a power distribution system.

In this article, a methodology to coordinate the legacy controllers and multiple DERs is designed and demonstrated. The main contribution of this article and the advantages of the proposed architecture are as follows.

1) The architecture is distributed and efficient and can integrate multiple DERs in the distribution system.
2) The methodology is computationally feasible and real-time implementable and, at the same time, can coordinate with local controllers of DERs.
3) The approach can be implemented considering any target location in the distribution system and is capable of working with regulators especially to avoid reverse power flow situations related to regulator malfunctions.
4) The approach can be applied to multiple target nodes in the distribution system simultaneously and maintain voltage stability and balance.

Compared to [26], the main contribution of this article is as follows.

1) The approach is evaluated for a large number of DERs with multiple target nodes.
2) The ability of the approach to coordinate with the distribution voltage regulators (DVRs) with large DERs is tested.
3) The optimal control algorithm is modified to scale up and, at the same time, coordinate with multiple DERs with multiple target nodes and voltage regulators.

The rest of this article is organized as follows. Section II discusses the overall proposed control architecture framework. Section III discusses the real-time modeling of the DER integrated power distribution systems. Section IV discusses the experimental setup and implementation results. Finally, Section V concludes this article.

II. Proposed Coordinated Control Architecture Using a Distributed Controller

In the proposed coordinated control architecture, an input–output signal-selection-based control using the ADMM is designed. Using measured data, a black-box transfer function model is estimated based on Lagrange multipliers [16], which is

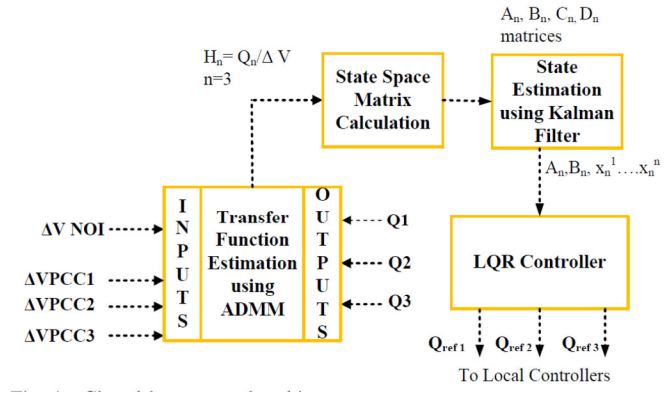

Fig. 1. Closed-loop control architecture.

further utilized to control reactive power and regulate the voltage at the node of interest. For estimating the transfer function model, first, the voltages and reactive powers are measured at the nodes of interest. Then, based on an ADMM-based optimization algorithm, the MIMO transfer function coefficient matrices A, B, C, and D are estimated. These matrices as then used to estimate the states based on a Kalman filter. Furthermore, an optimal controller is designed for each DER (note that the aggregated control outputs can also be estimated using this architecture) to find the required reactive power (Q) from DERs to support the voltage at the node(s) of interest.

As an example, the closed-loop control architecture depicted in Fig. 1 shows the reactive power outputs (Q_1, Q_2, and Q_3) from three DERs measured at the point of common coupling (PCC) and the deviation of target node voltage from a reference voltage (ΔV). These measurements are used to identify the transfer functions using the ADMM. The state-space matrices (A, B, C, and D) corresponding to each transfer function are then calculated (states and coefficients) using the ADMM and the Kalman filter. The states are then used to formulate the optimal control signals ($Qref1$, $Qref2$, and $Qref3$) for each DER to mitigate the voltage deviation. The reference signal generated is then sent to each DER.

A. ADMM-Based Transfer Function Identification

The ADMM is an optimization algorithm that combines the advantages of the dual ascent method and the method of multipliers. The optimization problem shown in (1) is solved with the primal variable split into two parts, x and z:

$$\begin{aligned} &\text{minimize} && f(x)+g(z) \\ &\text{subject to} && Ax+Bz=c. \end{aligned} \tag{1}$$

The augmented Lagrangian for optimization is developed similarly to the method of multipliers and is given by

$$\begin{aligned} L_\rho(x,z,y) = f(x)+g(z)+y^T(Ax+Bz-c) \\ +\frac{\rho}{2}||Ax+Bz-c||^2. \end{aligned} \tag{2}$$

The ADMM optimization routine consists of three main steps, i.e., an x-minimization step, a z-minimization step, and a dual-variable update step, as discussed in [27] and shown in

$$x^{k+1} := \underset{x}{\text{argmin}} L_\rho(x, z^k, y^k) \tag{3}$$

$$z^{k+1} := \underset{z}{\text{argmin}} L_\rho(x^{k+1}, z, y^k). \tag{4}$$

Constraints are handled as

$$y^{k+1} := y^k + \rho(Ax^{k+1} + Bz^{k+1} - c) \tag{5}$$

where ρ is the augmented Lagrangian parameter.

A method of identifying transfer functions using the ADMM is proposed in [28]. Based on this, the MIMO transfer function relating the deviation of voltage at a target node with the reactive power output from DERs can be written as

$$\begin{bmatrix}\Delta V\end{bmatrix} = \begin{bmatrix}H_1(z)\ H_2(z)\ H_3(z)\end{bmatrix} \begin{bmatrix}Q_1\\Q_2\\Q_3\end{bmatrix} \tag{6}$$

where ΔV is the deviation of the voltage from the reference voltage at a node of interest, and Q_1, Q_2, and Q_3 are the three-phase reactive power output of each DER.

The individual transfer functions (H_1, H_2, and H_3) in MIMO can be presented, and the parameters can be calculated as

$$H_1 = \frac{\Delta V}{Q_1} = \frac{b_0^1 + b_1^1 z^{-1} + \cdots + b_k^1 z^{-k}}{1 + a_1^1 z^{-1} + a_2^1 z^{-2} + \cdots + a_k^1 z^{-k}} \tag{7}$$

$$H_2 = \frac{\Delta V}{Q_2} = \frac{b_0^2 + b_1^2 z^{-1} + \cdots + b_k^2 z^{-k}}{1 + a_1^2 z^{-1} + a_2^2 z^{-2} + \cdots + a_k^2 z^{-k}} \tag{8}$$

$$H_3 = \frac{\Delta V}{Q_3} = \frac{b_0^3 + b_1^3 z^{-1} + \cdots + b_k^3 z^{-k}}{1 + a_1^3 z^{-1} + a_2^3 z^{-2} + \cdots + a_k^3 z^{-k}}. \tag{9}$$

Here $a_1, a_2, ..., a_k$ are the denominator coefficients of the transfer functions and $b_0, b_1, ..., b_k$ are the numerator coefficients of the transfer functions. From this, a global consensus optimization problem can be formulated as

$$\min_{a^1,\ldots,a^n} \frac{1}{2}|||[L][a] - [S] + [M][b]||^2 \tag{10}$$

where a and b are the vectors of all the denominator and numerator coefficients, respectively, S is the matrix of the current samples of ΔV, L is the matrix of the previous samples of ΔV, and M is the matrix of the current and previous samples of Q_1, Q_2, and Q_3.

With this, the state-space matrices (A, B, C, and D) are calculated from identified coefficients of each transfer function. For example, from (7)–(9), the state-space representations of H_1, H_2, and H_3 can be derived as A_{11}, B_{11}, A_{22}, B_{22}, A_{33}, and B_{33}. In addition, an array for ΔV (respective node voltage of interest, DERs of interest, and the regulator outputs as interest) as y and that of Q (reactive power inputs for DERs) as U can be deduced.

B. Kalman-Filter-Based State Estimation

The states of the system are estimated with a Kalman filter using state-space matrices and output measurement. The states

Algorithm 1: Kalman State Estimation.

Define $\hat{X}_{ke}$, P_{ke}, Q_{ke}, K_{ke}, R_{ke}, Res.
From grid measurements store U and y arrays respectively.
At discrete time instant k, develop A_{11}, and B_{11}, using ADMM algorithm.
Calculate estimated states $\hat{X}_{ke}$ from (11)
for $k = 1 : n_L$ **do**
    Project the state ahead using (12)
    Project the error co-variance estimate (13)
    for $k = 1 : n_L$ **do**
        Compute the Kalman gain using (14)
        Compute the measurement residue using (15)
        Update the state covariance matrix using (16)
        Update the error covariance estimate using (17)
    end
end
$\hat{X}(k+1) = A_{11}(k+1) \cdot \hat{X}(k) + B_{11}(k) \cdot U(k)$
return

are calculated from the measurement as

$$\hat{X}_{ke}(k) = A_{11}(k) \cdot \hat{X}_{ke}(k-1) + B_{11}(k) \cdot U(k). \tag{11}$$

Updates of the state ahead, error covariance matrices, Kalman gain, measurement residue, state covariance matrix, and error covariance matrix can be calculated as follows:

$$\hat{X}_{ke}(k+1) = A_{11}(k+1) \cdot \hat{X}_{ke}(k) + B_{11}(k) \cdot U(k) \tag{12}$$

$$P_{ke}(k+1) = A_{11}(k+1) \cdot P_{ke}(k) \cdot A_{11}^T(k) + Q_{ke} \tag{13}$$

$$K_{ke}(k) = \frac{P_{ke}(k) \cdot C_{11}^T(k)}{C_{11}(k) \cdot P_{ke}(k) \cdot C_{11}^T(k) + R_{ke}} \tag{14}$$

$$Res(k) = y(k) - C_{11}(k) * \hat{X}_{ke}(k) \tag{15}$$

$$\hat{X}(k+1) = \hat{X}_{ke}(k) + K_{ke}(k) \cdot Res(k) \tag{16}$$

$$P_{ke}(k) = [I - K_{ke}(k) \cdot C_{11}(k)] \cdot P_{ke}(k). \tag{17}$$

Finally, an updated state-space representation can be calculated. Algorithm 1 provides the overall approach.

C. Optimal Controller Design

Let the system model developed from the ADMM architecture along with the Kalman filter for one DER, represented as $(*_{11})$ can be written as

$$\hat{X}(k+1) - \hat{X}^*(k+1) = A_{11}(\hat{X}(k) - \hat{X}^*(k)) + B_{11}(k)(U(k) - U^*(k)) \tag{18}$$

where $\hat{X}(k+1)$ is a state vector, A_{11} is the state transition matrix, B_{11} is the input matrix, U is the control (or input) vector, and $(*)$ represents the certainly equivalence value.

The linear component of the system can be incorporated into the state transition matrix as follows:

$$\begin{bmatrix} \hat{X}_{k+1} \\ U_{k+1} \end{bmatrix} = \begin{bmatrix} A_{11} & B_{11} \\ 0 & 1 \end{bmatrix} \begin{bmatrix} \hat{X}_k \\ U_{k-1} \end{bmatrix} + \begin{bmatrix} B_{11} \\ I \end{bmatrix} \begin{bmatrix} \Delta U_k \end{bmatrix}. \tag{19}$$

The state space can then be rewritten as

$$\tilde{\hat{X}}(k+1) = A_{11}\tilde{\hat{X}}(k) + B_{11}U_{k-1} + B_{11}\Delta U_k \tag{20}$$

where $\sim$ represents the state error. From the above, a cost function can be defined for the optimal control as follows:

$$F(\hat{X}'_k, U, k) = \sum_{n=1}^{H} (\hat{X}_k - \hat{X}_k^\star)^T Q'(\hat{X}_k - \hat{X}_k^\star) + U^T(k) R' U(k)) \tag{21}$$

where $Q' = \begin{bmatrix} Q' & 0 \\ 0 & Q' \end{bmatrix}$ and R' is the penalty for change in controls.

Assuming that there is an uncertain component in the control (mainly due to noise and other system level changes), suboptimal control at previous time, and/or penalty factor (Q and R) variations, the control signal U is divided into nominal and uncertain U as

$$U = U^N + U^U \tag{22}$$

where U is the current control vector, and U^N and U^U are certainty control and uncertain control signal, respectively. Minimizing $F(\hat{X}'_k, U, k)$ in (21) can be achieved by finding an optimal policy related to state matrix $\pi(x)$ such that

$$\pi(x) = K_i * \hat{X}'_k. \tag{23}$$

The control parameter is adjusted using

$$K_i = -(R'_{H-i} + B_{11H-i}^T P_{i-1} B_{11H-i})^{-1} B_{11H-i}^T P_{i-1} A_{11H-i} \tag{24}$$

where H is the horizon window and $i = 1, 2, 3$.

Similarly

$$P_i = Q'_{H-i} + K_i^T R_{H-i} K_i + (A_{H-i} + \tag{25}$$

$$B_{11H-i} K_i)^T P_{i-1} (A_{H-i} + B_{11H-i} K_i). \tag{26}$$

The overall architectural flowchart is shown in Fig. 2.

III. Real-Time DER Integrated Distribution System Modeling

For DER-integrated real-time distribution system modeling, the distribution system lines are modeled in three phases using a distributed parameter line model. Other than lines, the models include voltage regulators, inline transformers, and unbalanced loads. The substation is assumed as a rigid voltage source with infinite capacity. The loads are modeled as spot loads and distributed loads. Multiple DERs are integrated into IEEE test distribution systems developed in real-time simulator modeling software. The grid model is based on the IEEE 123-bus test feeder, which is an unbalanced and multiphase network.

A. Distribution Voltage Regulators

DVRs are generally used on the power distribution feeder along with distribution lines or connected to the substation. In the case of three-phase regulators, models of three single-phase regulators of Y type are developed. Regulators can either control

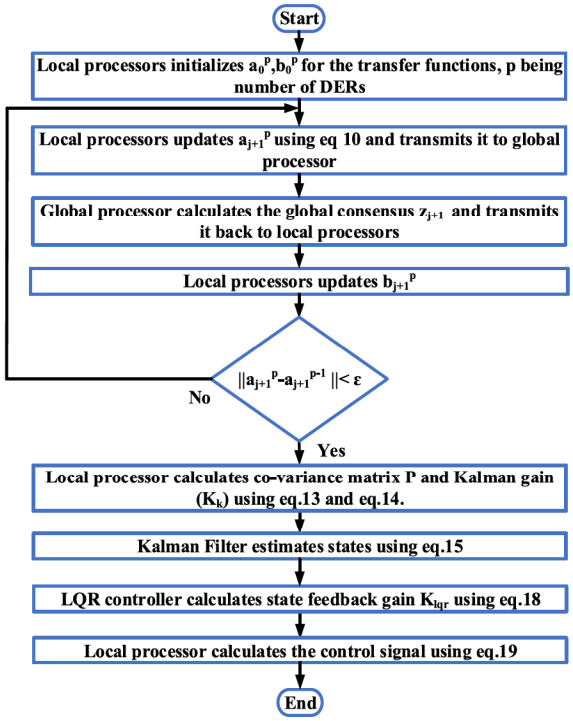

Fig. 2. Overall flowchart of the proposed architecture.

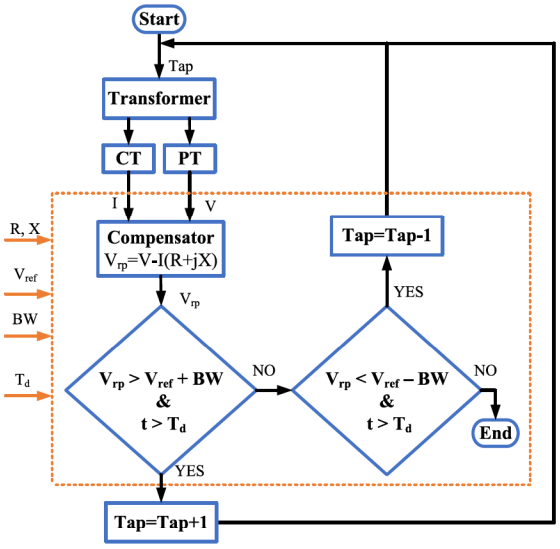

Fig. 3. Voltage regulator controller flow diagram.

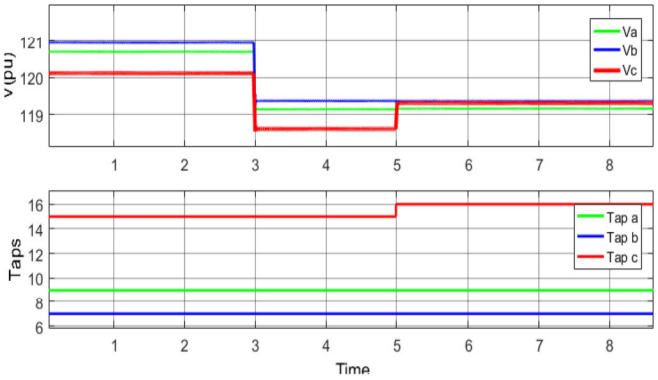

Fig. 4. Illustration of regulator tap operation.

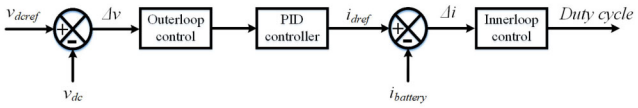

Fig. 5. Local control topology.

the voltage at its output node or control the voltage at a remote node downstream. A line drop compensator is used to regulate the voltage at a remote node. The compensator circuit has R and X settings, voltage-level setting (V_{ref}), bandwidth (BW) setting, and time delay (T_d) setting. The R and X settings are generally per unitized based on the line impedance seen from the regulation point and the regulator output. The voltage setting provides the desired regulator set points. The bandwidth provides the allowed deviation of the voltage from the regulation and the desired voltage set point. The time delay provides the time before the regulator action is being taken when the voltage falls outside the bandwidth. When the voltage at the remote node is higher than the upper voltage level setting $V_{\text{ref}} + BW$ and it stays there for a time greater than T_d, a raise operation is initiated and tap is increased. This process is continued until the tap reaches its maximum limit. Similarly, when the voltage at the remote node is lower than the lower voltage level setting $V_{\text{ref}} - BW$ and it stays there for a time greater than T_d, a lower operation is initiated and tap is decreased, as shown in Fig. 3. The developed regulator model is validated using a dynamic load variation. Fig. 4 illustrates a verification example in which a load is added to the IEEE 13-node test feeder in 3 s resulting in a voltage drop. The regulator taps raise after a delay of 2 s, as shown in Fig. 4. The voltage on phase C goes out of bounds. Therefore, a tap change occurs in regulator C, and with that, the voltage comes back to within the voltage range (band).

B. DER Integration to Distribution Grid

DER models that consist of PV farms with ratings of 350 kW, 1 MW, and 2 MW are designed for both 4160- and 24 900-V voltage levels. Design parameters of the 1-MW PV farm are shown in Table I. The PV array is connected to the grid through a dc–dc boost converter and a three-phase three-level voltage-source converter (VSC). Maximum power point tracking is implemented in the boost converter using a perturb and observe technique. The VSC converts the 500-V dc-link voltage to 260 V ac. The VSC control system uses two control loops: an external control loop that regulates the dc-link voltage to 500 V and an internal control loop that regulates I_d (active current component) and I_q (reactive current components) grid currents. I_d current reference is the output of the dc voltage external controller. The output of the current controller is voltages V_d and V_q, which are converted to three modulating signals for the inverter. The control topology is shown in Fig. 5.

The voltage at the PCC and nodes nearby would see a rise due to PV integration. Since there is no explicit control of voltage

TABLE I
DER DESIGN PARAMETERS

PV PLANT DESIGN			
Parameter	**Value**	**Parameter**	**Value**
Power Rating (MW)	2	PV Module	SunPower SPR-305E-WHT-D
AC Voltage (V, L-L)	480	Plant Output Voltage (Volts)	820.5
PV Plant Output Voltage (V)	820.5	Approximate Sting Voltage	820
Modulation Index, Ma	0.7838	Number of Modules in String NM	10
Voltage at the MPP, V_{mpp}	54.7	String Power SP (MW)	0.00305226
Current at the MPP, I_{mpp}	5.58	String Voltage, SV	820
Power at the MPP, P_{mpp}	305.226	Number of Strings, NS	437
Open-circuit voltage, V_{oc}	64.2	Number of arrays, NA	15
Short-circuit current, I_{sc}	5.96	Total Number of Modules, TNM	4370
Module Efficiency (%)	16.4	Array Power Rating (MW)	2
BATTERY DESIGN			
Parameter	**Value**	**Parameter**	**Value**
Power Rating (MWh)	1.2	Type	Lithium Ion
Maximum Capacity (Ah)	2000	Nominal Voltage (V)	600
Cutoff Voltage (V)	450	Fully Charged Voltage (V)	698
INVERTER DESIGN			
Parameter	**Value**	**Parameter**	**Value**
Average Model ac frequency (Hz)	60	Inverter Input DC Voltage V_{in} (V)	1000
Inverter Power Rating (MW)	2	Interfacing Capacitor C_{dc}	0.0798
Number of Inverters, NI	1	Acceptable Voltage Ripple (%)	5
Switching Frequency f_{sw} (kHz)	10	Inverter Output Voltage V_{out} (V,L-L)	480
Frequency Modulation Index Mf	90	DC Power P_{dc} (MW)	3
Id	5103.724	Em	391.9183588
Series Inductor Filter L_{ac}	0.15		
DC BOOST CONVERTER DESIGN			
Parameter	**Value**	**Parameter**	**Value**
Average Model Number of Converters	1	Converter Inductor L_{conv} (mH)	0.1208
Converter Input Voltage, V_{in}	820	Converter Input Capacitor C_{conv} (μF)	1100
Converter Power Rating (MW)	2	Acceptable Current Ripple (%)	5
Converter Output Voltage, V_{out}	1000	Duty Cycle, D	0.1795

at the PCC, the voltage regulator would regulate the voltage by changing taps.

C. Coordination Between Local Controls of DERs

As discussed, the local control of the DERs is modeled as illustrated in Fig. 6. With the PV farm, if a battery energy storage is included, the inverter of the battery could be controlled to regulate the voltage at the node of interest. Here, the voltage at the node of interest is measured, and a reference for active and reactive power is generated for the inverter of the battery. Since the distribution system has a higher R/X ratio, the active power can also be used to regulate the voltage at a node if necessary. Therefore, either active power (ΔP control) or reactive power (ΔQ control) or both could be controlled to regulate voltage (ΔP + ΔQ control). For the coordination control architecture, the control topology in Fig. 5 is extended to add reactive power outer loop to the ΔV control. The integration framework of the proposed architecture with the DER-enabled power distribution network is shown in Fig. 6. As can be seen from Fig. 6, the proposed architecture serves as an outer loop to the dq control framework integrated as the local controller for the PV–battery system and collect information from the grid based on measurements. In this article, all the DERs are considered to operate in the grid-connected mode. The DER active power set point (P) is left uncontrolled with the proposed controller. The reactive power set point is generated by the proposed controller to regulate the voltage at the node of interest.

D. Implementation With the OPAL-RT Real-Time Simulator

The full model that includes distribution systems with DERs integrated is built to run in real time using a real-time simulator called Opal-RT simulator. A software-in-the-loop real-time simulation approach [29] is utilized, where both the controller and plant models run on the same simulator. In the RT-Lab, the ARTEMiS-SSN solver is specifically designed for microgrid and distribution systems that provide fast and accurate real-time simulation without introducing artificial delays [30]. The method used to model the power grid in this architecture is known as the state-space nodal method, which virtually decouples the system into subsystems and then solves the system equations using the

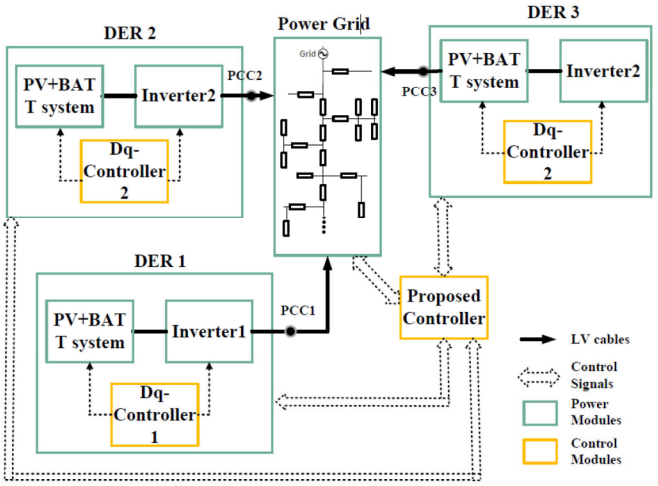

Fig. 6. Overall architecture of the system under study.

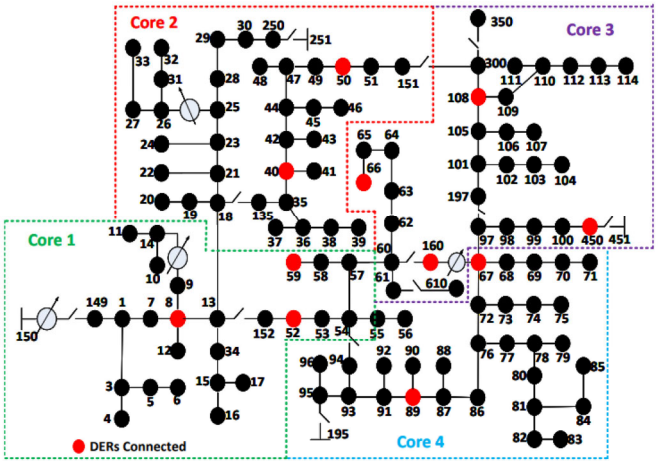

Fig. 8. One-line diagram of the IEEE 123-bus distribution test feeder with DERs modeled in a real-time simulator.

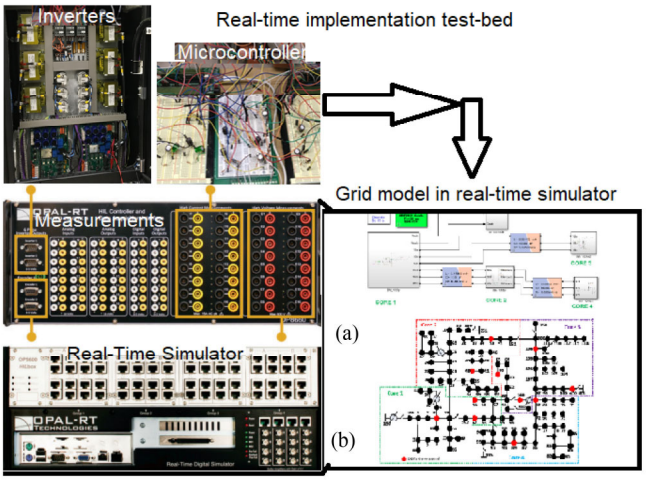

Fig. 7. Real-time implementation using the Opal RT Simulator.

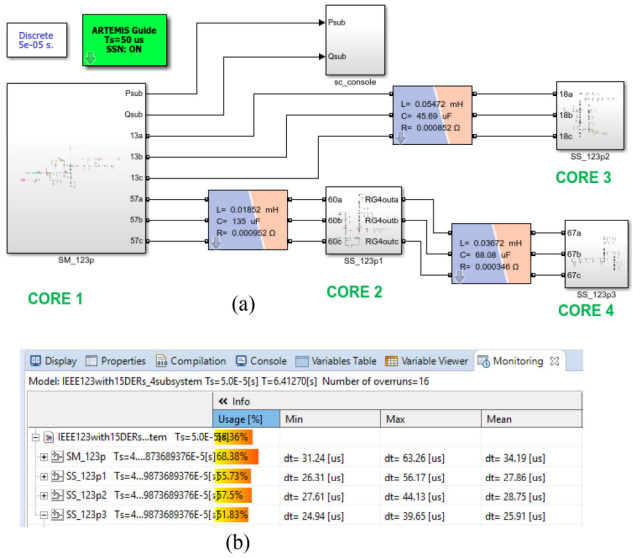

Fig. 9. (a) IEEE 123-bus distribution test feeder with DERs in Opal RT. (b) Core Usage of Opal RT.

nodal admittance method. For the proposed study, the models are initially created in Simulink, which has Opal-RT libraries. Then, the RT-Lab GUI is used to run the model in real time using a three-step process, namely, build, load, and execute. The build process converts the model into a Linux executable code. The load process uploads the executable code to the simulator, and the execute process starts the real-time simulation in the simulator, as shown in Fig. 7. The model is also verified with inverters [power hardware in the loop (HIL)], as discussed in Fig. 7. All the results are based on the real-time simulation and/or HIL tests.

In this article, the IEEE 123-bus system with multiple DERs is modeled to run in real time. The real-time simulator OP 5707 is used, which has 16 cores. The models are first designed in Simulink and then partitioned into multiple subsystems using ARTEMiS Stubline blocks [31], as shown in Fig. 8, to run it in different cores and leverage the parallel computing capability of the RT-Lab. To validate the robustness of the proposed control architecture, test feeders with another voltage level, such as IEEE 34-bus system, are also utilized. The computational burden and core usage for a 50-μs time step simulation are depicted in Fig. 9.

It can be seen that there are minimal overruns (close to zero), which validate the successful real-time execution of the model.

IV. Experimental Results With Real-Time Simulator

As mentioned, the overall architecture is tested on a real-life power grid model of IEEE 123-node test feeder developed in the real-time simulator. The feeder has four voltage regulators and one feeder head transformer. All the loads connected are unbalanced and have the ZIP configurations (constant impedance, power, and voltage). The feeder also have laterals, which can be used to test multiphase DERs. The model runs in 50-μs time step on the simulator. The power grid model is modified first to include DERs at specific nodes that are randomly selected. Five cases are considered for the proposed study. The first case tests the ability of the DERs to support the voltage at a node of interest by varying its reactive power output. The second case is used to study the voltage regulation on the feeder measured at

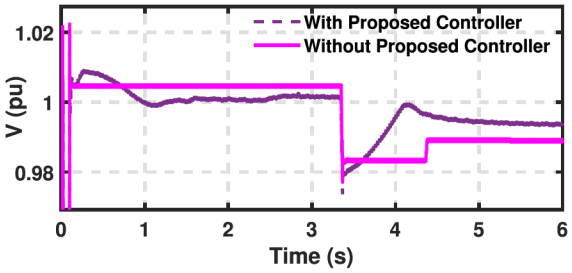

Fig. 10. Voltage variations at the point of interest node.

the regulator points and the effect of that on regulator taps. The third case illustrates DERs targeting voltages of multiple nodes of interest simultaneously. The fourth case studies the ill effects of DER location on-grid voltages and how the proposed method can be used to mitigate it, and the fifth case demonstrates the robustness of the proposed method when there is a loss of DERs. 350-kVA inverters are used for simulation in cases 1–3 and 5. For case 4, the coordinated control of the proposed architecture with DER and the regulator are tested. For this, the impact of large DER at end of the feeder is tested. Therefore, a combination of 2-MVA DERs (4 MVA total) is used. The reason is that large DER causes regulator maloperations. The test is to see if the proposed architecture can mitigate the regulator maloperation and subsequent voltage changes during the reverse power flow conditions. In all these cases, the active power set point is left uncontrolled with the proposed controller.

A. Case I: Voltage Support

The capability of the proposed architecture to maintain the voltage at the reference value for a particular node of interest is demonstrated in this test case. For this purpose, node 107 is considered the point of interest. The goal is to maintain the voltage at 1 p.u. Fig. 10 illustrates the change in the voltage when there is a sudden change in the load at 3 s. The voltage dips without the proposed architecture; however, the voltage was maintained almost the same with the proposed architecture. The area under the curve illustrates that a total improvement of 10% is achieved in the voltage support with the proposed architecture.

B. Case 2: Voltage Regulation and Tap Improvement

This case illustrates the coordination of the proposed architecture with legacy voltage regulator controllers for balancing the DER reactive power support to improve the voltage at the target node and, at the same time, balancing the voltage regulator tap operation. For this purpose, a test case is developed with a load variation at the point of interest, as shown in Fig. 11(a), which results in the voltage variation at that node. The tap control discussed in Section III-A is designed and implemented for this purpose. The tap control delay is set at 1 s, so it can be seen that the taps are initiated at 1 s after the load change has occurred. The taps continue to operate until the voltages are within the range of the voltage set point of the regulator. The voltage change based on the regulator action is illustrated in Fig. 11(b).

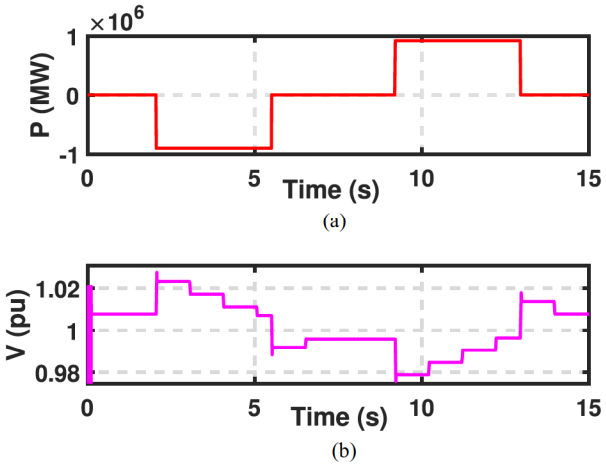

Fig. 11. (a) Load variation. (b) Voltage variation at node 197 with load variation and regulator tap action.

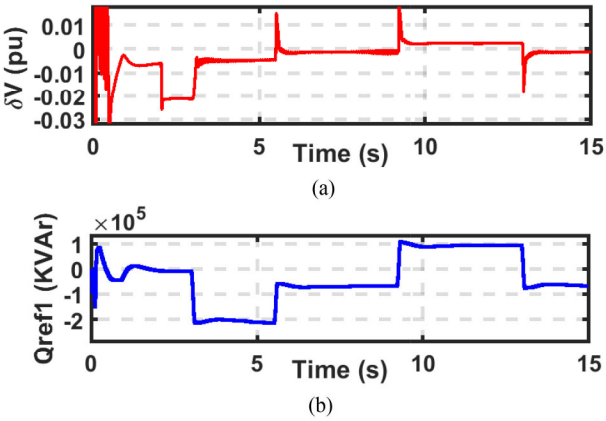

Fig. 12. (a) Voltage deviation ΔV at target node 197. (b) Reactive power reference of DER 1.

Next, the capability of the proposed controller action on maintaining the voltage at the targeted node and, at the same time, balancing the regulator action is illustrated. For this, three DERs each rated 350 kVA are utilized to regulate the voltage at a target node. The locations of DERs are bus 450, 67, and 10, respectively. Fig. 12(a) illustrates the change in the voltage from a reference voltage at the targeted node (node 197) with the proposed architecture. It can be seen that based on the reactive power reference developed with the proposed distributed control architecture [see Fig. 12(b)], the change in the voltage from a reference voltage is maintained close to zero; in other words, the voltage is maintained close to the reference voltage. Note that the controller action is initiated at 3 s to demonstrate the effect on the voltage with and without the proposed controller (before and after 3 s). It can also be seen that the reactive power is absorbed and delivered as required from the DERs. From the figures, it can also be noted that the deviations in the voltage are used to generate the right reactive power (positive for improving the voltage and negative for reducing the voltage), so the architecture works in a closed loop based on measurements. The tap operations of one voltage regulator at bus 160-67 are illustrated in Fig. 14. It can be noted that the tap operations are

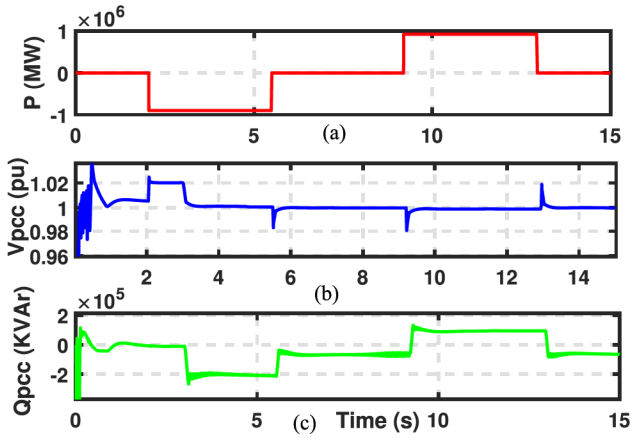

Fig. 13. (a) Load variation. (b) Voltage at the PCC of DER1. (c) Reactive power at the PCC of DER 1.

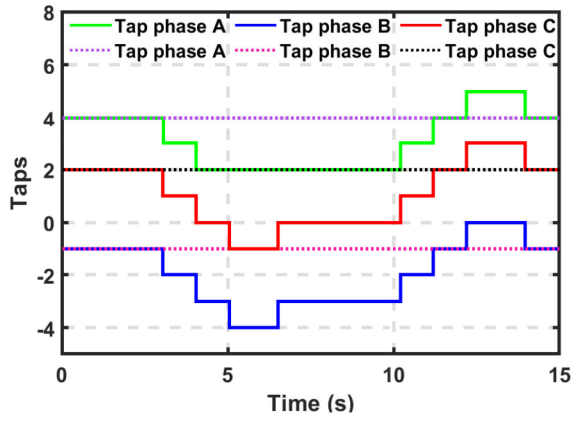

Fig. 14. Taps operation of regulator 160-67.

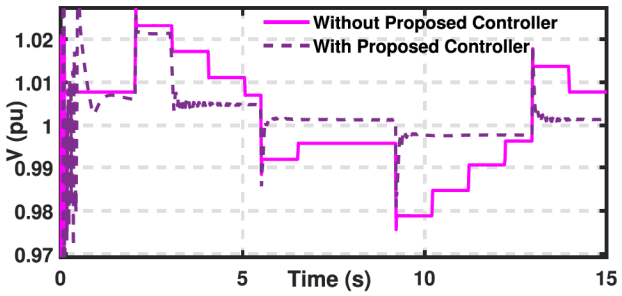

Fig. 15. Voltage comparison at target node 197.

reduced to zero from 21 taps overall. The delay settings of the regulator tap are the same as before (1 s).

It can be seen from Fig. 15 that with the proposed architecture, the voltages are regulated much better with the zero-tap operation of the regulator with an overall improvement of 11% in the voltage deviations and 21 tap reduction in the regulator taps.

C. Case 3: Demonstration of Multiple DERs Targeting Multiple Nodes of Interest Simultaneously

Several scenarios are used to test the efficacy of the proposed controller with multiple DERs and multiple points of interest.

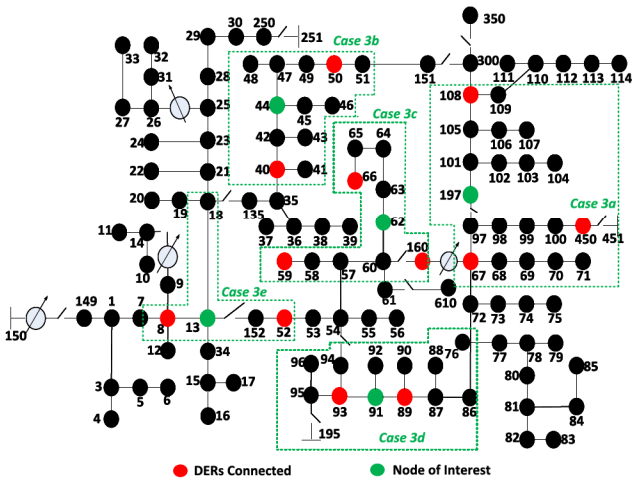

Fig. 16. Location of DERs.

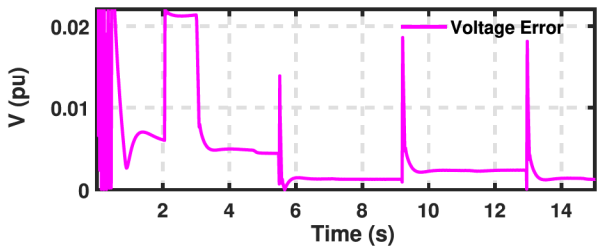

Fig. 17. Voltage error at target node for case 1.

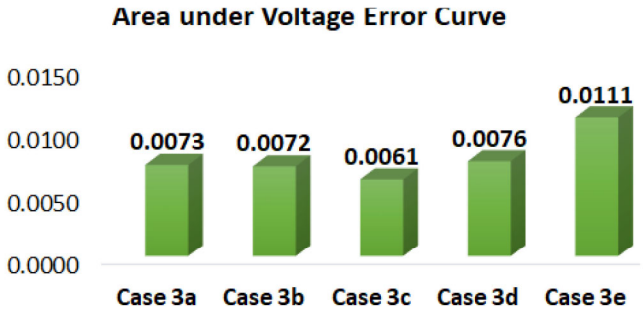

Fig. 18. Voltage error area comparison for different cases.

Additional tests done based on the study and the location of DERs for each test case are shown in Fig. 16, in which a group of DERs connected to different nodes of the IEEE 123-bus system is used to regulate the voltage of a target node. Switches 13-152, 60-160, and 97-197 are in close position. The effectiveness of the controller to regulate voltage close to a reference voltage is obtained by calculating the area under the voltage error curve, as shown in Fig. 17. The comparison of area for different test cases is depicted in Fig. 18. It can be concluded from Fig. 18 that the voltage error area is almost the same for all the cases. Thus, it can be concluded that the controller is capable of regulating target node voltages irrespective of the location of the DER in the feeder. Table II illustrates the cases and the voltage improvement comparisons.

TABLE II
TEST SYSTEMS AND VOLTAGE IMPROVEMENT

Sl No	Test Cases	Number of DERs	Number of Nodes	Node of Interest	Error Improvement (in %)
1	Case 3a	3	20	197	29.22
2	Case 3b	2	12	44	30.14
3	Case 3c	3	10	62	36.45
4	Case 3d	1	12	91	27.45
5	Case 3e	2	6	13	19.45

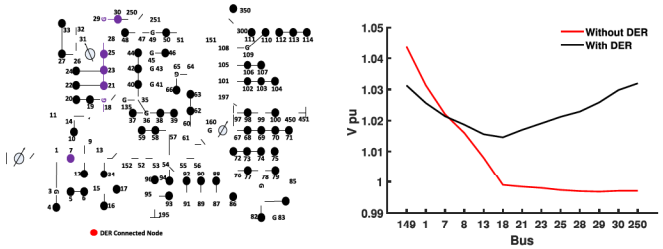

Fig. 19. (a) DER far from the substation. (b) Phase A voltage profile.

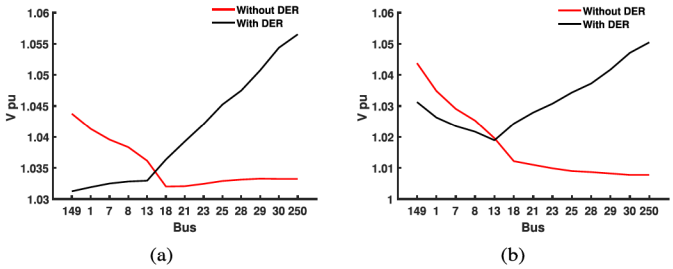

Fig. 20. (a) Phase B voltage profile. (b) Phase C voltage profile.

D. Case 4: Impact of DER Location on Operation of Voltage Regulators and Adverse Effect Mitigation With the Proposed Architecture

The location of large DERs will have an impact on voltage regulating devices as well as grid voltages. If the DER injects power just downstream from the voltage regulator, customers at the end of the line will experience low voltage, and if DER injects power at the end of the feeder (remote node), high voltage may occur at the remote node [32]. In this case, the location of DERs from the substation and how it impacts the operation of voltage regulating devices are studied. Then, the effect of the proposed architecture to mitigate the effect of inadequate regulator operations is illustrated. First, a large DER operating at unity power factor is connected to a remote node from substation (node 250), as shown in Fig. 19(a). When the power of 4 MW is injected, the PCC, as well as other nearby nodes, would experience a high voltage. The voltage regulator performs tap-down operations until the regulating point voltage is within the bandwidth. Even though the regulating point voltage is close to the reference voltage, the remote node where DER is connected can still have a higher voltage profile due to high DER penetration. The three-phase voltages of nodes (shown in violet color) from the substation to the remote node is depicted in Figs. 19(b), 20(a), and 20(b). It can be seen that, with high

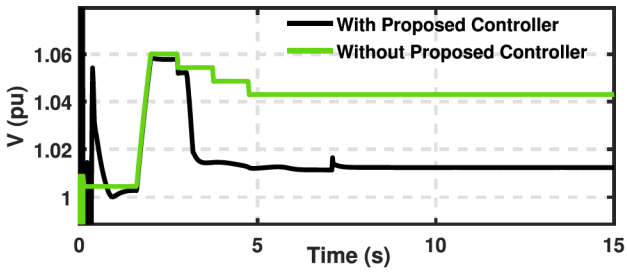

Fig. 21. Voltage comparison at remote node 250 with large DERs.

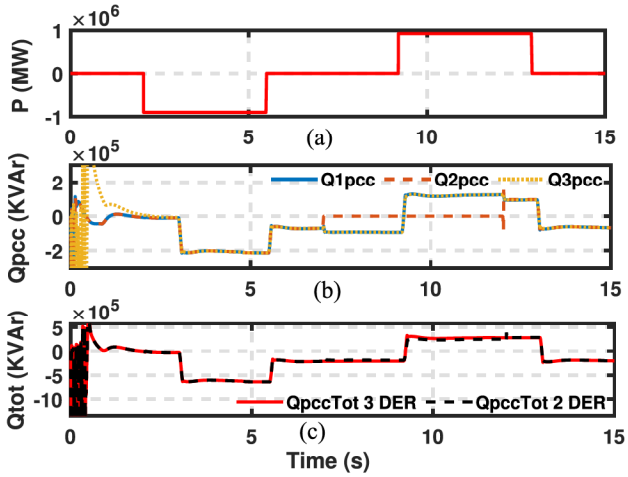

Fig. 22. (a) Load variation. (b) Reactive power of each DER. (c) Total reactive power from DERs.

DER penetration at a remote node of the feeder, nodes toward the end of the feeder would experience a higher voltage profile even after the operation of voltage regulators.

In order to improve the voltage profile at remote node, the proposed control methodology is used. It can be seen from Fig. 21 that with the proposed control, the voltages are closer to 1 p.u., whereas without control, the voltages are closed to 1.05 p.u. even after the operation of the regulator.

E. Case 5: Loss of DERs

In this case, the effectiveness of the controller during a condition with the sudden loss of one or more DERs is studied. Three DERs each rated 350 kVA are utilized for reactive power support to regulate the voltage at node 197 to 1 p.u. The location of DERs is bus 450, 67, and 105, respectively. The DER 2 is taken out at 7 s and brought back at 12 s. The reactive power contribution from DER 2 falls to zero at 7 s and comes back at 12 s, as shown in Fig. 22(b). The tertiary controller dynamically changes the output of the other two DERs during this time. The output from DERs 1 and 3 are increased at 7 s as soon as DER 2 is lost and DER 1 and 3 outputs are reduced as soon as DER 2 comes back at 12 s, as shown in Fig. 22(b). In addition, it can be seen from Fig. 22(c) that the total reactive power of all the DERs remains almost the same due to this change. The voltage variation due to a load variation at the target node is minimal and is maintained closer to the reference voltage even with the loss of one DER, as shown in Fig. 23.

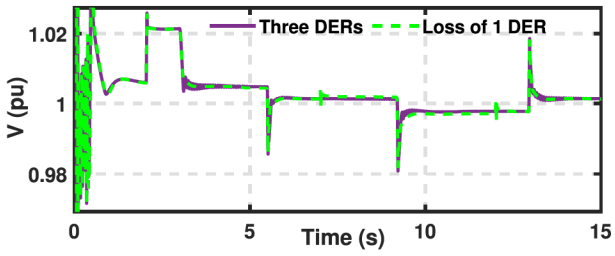

Fig. 23. Voltage comparison at target node 197.

V. Conclusion

In this article, a distributed coordinated control methodology was proposed that can be used to coordinate legacy controllers and IBR-based DERs. The case studies were performed with real-time simulators and field-implementable power grid feeders. The effectiveness of the algorithm was validated based on several case studies, such as: 1) providing sufficient reactive power compensation to regulate the voltage at the point of interest; 2) coordinating with the legacy controllers; 3) developing a group of DERs and control voltage at multiple points of interests; 4) provides a framework to balance the voltage for utility-scale DERs; and 5) balance the voltage in the wake of the loss of DERs. It was observed that the proposed architecture not only performs well by mitigating the voltage deviation of more than 20% but can also support legacy controllers, such as voltage regulators, to reduce the number of taps and mitigate malfunction during reverse power flow situation. The future work will include control HIL and field implementation in the microgrid scenarios of the proposed method.

References

[1] M. A. Hossain, H. R. Pota, W. Issa, and J. Hossain, "Overview of ac microgrid controls with inverter-interfaced generations," *Energies*, vol. 10, 2017, Art. no. 1300.

[2] W. Sheng, K.-y. Liu, S. Cheng, X. Meng, and W. Dai, "A trust region SQP method for coordinated voltage control in smart distribution grid," *IEEE Trans. Smart Grid*, vol. 7, no. 1, pp. 381–391, Jan. 2016.

[3] X. Su, M. A. S. Masoum, and P. J. Wolfs, "Multi-objective hierarchical control of unbalanced distribution networks to accommodate more renewable connections in the smart grid era," *IEEE Trans. Power Syst.*, vol. 31, no. 5, pp. 3924–3936, Sep. 2016.

[4] V. Kekatos, G. Wang, A. J. Conejo, and G. B. Giannakis, "Stochastic reactive power management in microgrids with renewables," *IEEE Trans. Power Syst.*, vol. 30, no. 6, pp. 3386–3395, Nov. 2015.

[5] A. Newaz, J. Ospina, and M. O. Faruque, "Coordinated voltage control in distribution systems with distributed generations," in *Proc. IEEE Power Energy Soc. Gen. Meeting*, 2019, pp. 1–5.

[6] B. A. Robbins and A. D. Domínguez-García, "Optimal reactive power dispatch for voltage regulation in unbalanced distribution systems," *IEEE Trans. Power Syst.*, vol. 31, no. 4, pp. 2903–2913, Jul. 2016.

[7] P. Šulc, S. Backhaus, and M. Chertkov, "Optimal distributed control of reactive power via the alternating direction method of multipliers," *IEEE Trans. Energy Convers.*, vol. 29, no. 4, pp. 968–977, Dec. 2014.

[8] H. J. Liu, W. Shi, and H. Zhu, "Distributed voltage control in distribution networks: Online and robust implementations," *IEEE Trans. Smart Grid*, vol. 9, no. 6, pp. 6106–6117, Nov. 2018.

[9] L. Wang, F. Bai, R. Yan, and T. K. Saha, "Real-time coordinated voltage control of PV inverters and energy storage for weak networks with high PV penetration," *IEEE Trans. Power Syst.*, vol. 33, no. 3, pp. 3383–3395, May 2018.

[10] T. Sansawatt, L. F. Ochoa, and G. P. Harrison, "Smart decentralized control of DG for voltage and thermal constraint management," *IEEE Trans. Power Syst.*, vol. 27, no. 3, pp. 1637–1645, Aug. 2012.

[11] A. G. Madureira and J. A. P. Lopes, "Coordinated voltage support in distribution networks with distributed generation and microgrids," *IET Renewable Power Gener.*, vol. 3, no. 4, pp. 439–454, Dec. 2009.

[12] K. Alobeidli and M. S. E. Moursi, "Novel coordinated secondary voltage control strategy for efficient utilisation of distributed generations," *IET Renewable Power Gener.*, vol. 8, no. 5, pp. 569–579, 2014.

[13] J. Miret, A. Camacho, M. Castilla, L. G. de Vicuña, and J. Matas, "Control scheme with voltage support capability for distributed generation inverters under voltage sags," *IEEE Trans. Power Electron.*, vol. 28, no. 11, pp. 5252–5262, Nov. 2013.

[14] F. A. Viawan and D. Karlsson, "Combined local and remote voltage and reactive power control in the presence of induction machine distributed generation," *IEEE Trans. Power Syst.*, vol. 22, no. 4, pp. 2003–2012, Nov. 2007.

[15] A. Thakallapelli and S. Kamalasadan, "Measurement-based wide-area damping of inter-area oscillations based on MIMO identification," *IET Gener. Transmiss. Distrib.*, vol. 14, pp. 2464–2475, 2020.

[16] A. Thakallapelli and S. Kamalasadan, "Alternating direction method of multipliers (ADMM) based distributed approach for wide-area control," in *Proc. IEEE Ind. Appl. Soc. Annu. Meeting*, 2017, pp. 1–7.

[17] S. Abdelrazek, S. Kamalasadan, J. Enslin, and T. Fenimore, "Integrated optimal control of battery energy storage management system for energy management and PV capacity firming," in *Proc. IEEE Energy Convers. Congr. Expo.*, 2015, pp. 62–69.

[18] M. Ahmed and S. Kamalasadan, "An approach for local net-load ramp rate control using integrated energy storage based on least square error minimization technique," in *Proc. IEEE Power Energy Conf. Illinois*, 2018, pp. 1–6.

[19] L. Wang, A. Dubey, A. H. Gebremedhin, A. Srivastava, and N. Schulz, "MPC-based decentralized voltage control in power distribution systems with EV and PV coordination," *IEEE Trans. Smart Grid*, vol. 13, no. 4, pp. 2908–2919, doi: 10.1109/TSG.2022.3156115.

[20] W. Zhong, G. Tzounas, and F. Milano, "Improving the power system dynamic response through a combined voltage-frequency control of distributed energy resources," *IEEE Trans. Power Syst.*, early access, doi: 10.1109/TPWRS.2022.3148243.

[21] A. M. d. S. Alonso, L. De Oro Arenas, D. Brandao, E. Tedeschi, and F. P. Marafao, "Integrated local and coordinated overvoltage control to increase energy feed-in and expand DER participation in low-voltage networks," *IEEE Trans. Sustain. Energy*, vol. 13, no. 2, pp. 1049–1061, Apr. 2022.

[22] G. Fazelnia, R. Madani, A. Kalbat, and J. Lavaei, "Convex relaxation for optimal distributed control problems," *IEEE Trans. Autom. Control*, vol. 62, no. 1, pp. 206–221, Jan. 2017.

[23] R. Cheng, Z. Wang, Y. Guo, and Q. Zhang, "Online voltage control for unbalanced distribution networks using projected Newton method," *IEEE Trans. Power Syst.*, early access, doi: 10.1109/TPWRS.2022.3144246.

[24] M. Elsisi, M. Aboelela, M. Soliman, and W. Mansour, "Design of optimal model predictive controller for LFC of nonlinear multi-area power system with energy storage devices," *Electr. Power Compon. Syst.*, vol. 46, nos. 11/12, pp. 1300–1311, 2018.

[25] R. Bisht, S. Subramaniam, R. Bhattarai, and S. Kamalasadan, "Active and reactive power control of single phase inverter with seamless transfer between grid-connected and islanded mode," in *Proc. IEEE Power Energy Conf. Illinois*, 2018, pp. 1–8.

[26] A. Suresh, R. Bisht, and S. Kamalasadan, "ADMM based LQR for voltage regulation using distributed energy resources," in *Proc. IEEE Int. Conf. Power Electron., Drives Energy Syst.*, 2020, pp. 1–6.

[27] S. Boyd, N. Parikh, E. Chu, B. Peleato, and J. Eckstein, "Distributed optimization and statistical learning via the alternating direction method of multipliers," *Found. Trends Mach. Learn.*, vol. 3, no. 1, pp. 1–122, 2010.

[28] A. Thakallapelli and S. Kamalasadan, "Alternating direction method of multipliers (ADMMs) based distributed approach for wide-area control," *IEEE Trans. Ind. Appl.*, vol. 55, no. 3, pp. 3215–3227, May/Jun. 2019.

[29] J. Bélanger, P. Venne, and J.-N. Paquin, "The what, where and why of real-time simulation," *Planet Rt*, vol. 1, no. 1, pp. 25–29, 2010.

[30] H. Hooshyar, L. Vanfretti, and C. Dufour, "Delay-free parallelization for real-time simulation of a large active distribution grid model," in *Proc. 42nd Annu. Conf. IEEE Ind. Electron. Soc.*, 2016, pp. 6278–6284.

[31] H. Hooshyar, F. Mahmood, L. Vanfretti, and M. Baudette, "Specification, implementation, and hardware-in-the-loop real-time simulation of an active distribution grid," *Sustain. Energy, Grids Netw.*, vol. 3, pp. 36–51, 2015.
[32] D. Ton, G. H. Peek, C. Hanley, and J. Boyes, "Solar energy grid integration systems (SEGIS)," Sandia Nat. Lab., Tech. Rep., pp. 4–19, 2008.

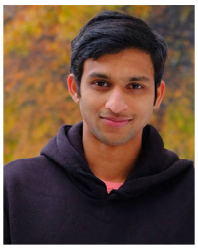

Arun Suresh (Student Member, IEEE) received the B.Tech. degree in electrical engineering from Mahatma Gandhi University, Kottayam, India, in 2012, the M.Tech. degree in electrical engineering from Kerala University, Thiruvananthapuram, India, in 2015, and the Ph.D. degree in electrical engineering from the University of North Carolina, Charlotte, NC, USA, in 2021.

He is currently a Consultant with Hitachi Energy, Raleigh, NC. His research interests include power system stability and control, smart grids, and integration of renewable energy in power systems.

Robin Bisht (Student Member, IEEE) received the B.Tech. degree in electrical and electronics from the Visvesvaraya National Institute of Technology, Nagpur, India, in 2013, and the M.Sc. degree in electrical and computer engineering in 2016 from the University of North Carolina, Charlotte, NC, USA, where he is currently working toward the Ph.D. degree in electrical engineering.

His research interests include microgrids, smart inverters, application of power electronics in power systems, and control of power systems.

Sukumar Kamalasadan (Senior Member, IEEE) received the B.Tech. degree in electrical and electronics engineering from the University of Calicut, Malappuram, India, in 1991, the M.Eng. degree in electrical power systems management from the Asian Institute of Technology, Bangkok, Thailand, in 1999, and the Ph.D. degree in electrical engineering from the University of Toledo, Toledo, OH, USA, in 2004.

He is currently a Professor with the Department of Electrical and Computer Engineering, University of North Carolina at Charlotte, Charlotte, NC, USA. His research interests include intelligent and autonomous control, power systems dynamics, stability, and control, smart grids, microgrids, real-time optimization, and control of power systems.

Dr. Kamalasadan was the recipient of several awards, including the National Science Foundation CAREER Award and the IEEE Best Paper Award.